



# State of health estimation of lithium-ion battery based on CNN–WNN–WLSTM

Quanzheng Yao<sup>1</sup> · Xianhua Song<sup>1</sup> · Wei Xie<sup>1</sup>

Received: 11 August 2023 / Accepted: 11 November 2023 / Published online: 6 January 2024  
© The Author(s) 2024

## Abstract

Accurate and stable estimation of the state of health (SOH), which is one of the critical indicators to characterize the ability of lithium-ion (Li-ion) batteries to store and release energy, is critical in the stable driving of electric vehicles. In this paper, a novel SOH estimation method based on the aging factors of battery, which combines convolutional neural network (CNN), wavelet neural network (WNN), and wavelet long short-term memory (WLSTM) named CNN–WNN–WLSTM, is designed. The proposed CNN–WNN–WLSTM estimation scheme inherits both the fast convergence and robust stability of the WNN, as well as the ability of long short-term memory neural network (LSTM) to extract the time series features of the data; moreover, using CNN can make the proposed algorithm extract the data features from the original battery data automatically, and the WNN–WLSTM is then adopted to produce the final SOH estimation by exploiting the features from the CNN. To further speed and achieve global optimization, the RMSprop optimizer, instead of the usually used Adagrad optimizer, is chosen as the solver of the CNN–WNN–WLSTM network. Experimental results on data set from the NASA Ames Prognostics Center of Excellence show that the proposed algorithm can be commendably used for Li-ion battery health management by quantitative comparison with other commonly used machine learning methods, such as back-propagation neural network, WNN, LSTM, WLSTM, convolutional neural network–long short-term memory neural network (CNN–LSTM), and Gaussian process regression.

**Keywords** Lithium-ion batteries · State of health · Convolutional neural network · Wavelet neural network · Wavelet long short-term memory

## Introduction

Li-ion batteries are the primary energy sources for electric vehicles because of their advantages of lightweight, long life, high efficiency, and low cost [1–4]; thus, the performance evaluations of lithium batteries are of great significance for the practical use of electric vehicles. Typically, lithium batteries are regulated and evaluated using battery management system (BMS) [5–7]. The evaluation indexes of BMS mainly consist of State of Charge (SOC), Remaining Useful Life (RUL), and SOH [8–12]. Generally, SOH describes long-term changes, so it is vital to obtain accurate SOH estimations for the long-term safe and stable use of batteries.

✉ Xianhua Song  
songxianhua@hrbust.edu.cn

<sup>1</sup> School of Science & Heilongjiang Provincial Key Laboratory of Optimization Control and Intelligent Analysis for Complex Systems, Harbin University of Science and Technology, Harbin, China

To date, numerous estimation methods have been proposed, and they can be generally divided into three types: direct calibration methods, model-based methods, and data-driven approaches. A typical direct calibration is the accumulating current integration [13–16]. However, in practice, this method is easily affected by the sampling precision of the current, and the results in the application cannot work well. Electrochemical impedance spectroscopy (EIS) is another direct method [17–19], which obtains the chemical states inside the battery by analyzing the ac impedance spectrum of the battery at different frequencies. Then, the exterior features of the battery are evaluated. However, the collection of internal battery parameters requires special and expensive equipment. The model-based method first uses electrochemical model to model the battery, and then uses model parameters to achieve the SOH estimation [20]. However, it is difficult to choose a suitable model to balance the estimation accuracy and computational complexity. The last

mainstream method is data-driven, which depicts the battery performance from the perspective of the experimental data. It discovers the hidden information to estimate the SOH through all kinds of data learning modes and does not need the knowledge of the battery systems. Therefore, this method can avert the difficult problem of model obtainment.

As a common data-driven algorithm, support vector machine (SVM) estimates SOH by mapping non-linear problems in low-dimension space to linear problems in higher dimension space [21, 22]. This method has low computational complexity and strong training ability for a small amount of sample data. However, it is difficult to choose the proper kernel function and is highly dependent on cross-training and regularization methods. The relevance vector machine (RVM) is roughly the same as that of SVM, but the network weights are obtained using the sparse Bayesian theoretical structure [23, 24], so the output is probability density estimation rather than point estimation. However, due to the sparse matrix of the RVM model, the demand for training data is relatively high, and the stability of the estimation results is poor. GPR is also an estimation method for regression analysis of system behavior processes based on the Bayesian framework and prior knowledge [25]. However, there are many hyper-parameters in this algorithm, so the process of adjusting the hyper-parameters during training is cumbersome. As efficient data-driving methods, neural network-based methods are becoming the mainstream methods in battery performance evaluations [26–35]. Among them, the WNN combines the ability of self-learning and non-linear function approximation, so it has the advantages of high accuracy and the ability of detailed depiction, which make WNN preponderance in the realm of SOH estimation [36, 37]. Zhang et al. proposed a four-layer WNN, which combines discrete wavelet multiresolution decomposition with multi-layer perceptron, and it has better predictive performance compared with BPNN. However, this method is restricted to multiresolution analysis, so its structure is not flexible and its robustness is not strong [38]. Xia et al. adjusted the network structure of WNN by introducing the wavelet dilation parameter and the wavelet translation parameter, which gives the network the advantage of strong robustness [39]. However, it is only a three-layer neural network, so its estimation accuracy is far less than that of deep networks. Compared with BPNN, the recurrent neural network (RNN) [40] has been used in estimating SOH, because it can save the important information between the input data and the SOH value. However, RNN cannot be used for long-term estimation due to the problems of vanishing gradients and exploding gradients. To address this issue, LSTM is introduced [41–44]. The LSTM has the unit state that can save the most important information between the input and output. However, because of the characteristic of the LSTM cell,

its robustness is not strong when the correlation between the testing data and the training data is not high.

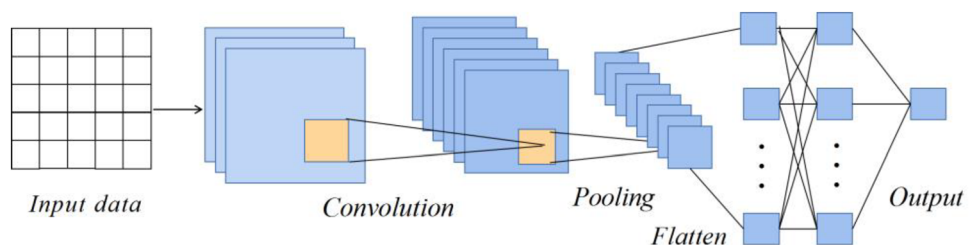
The feature extraction of input data, which is based on the aging factors of battery, is a commonly and important problem for SOH estimation [45–49]. Yang et al. extracted four data features from the constant current–constant voltage (CC–CV) charging curve of battery [50]. However, some features are difficult to extract, such as the slope of the curve at the end of CC charging mode and the vertical slope at the corner of the CC charging curve. Thus, extracting the data features manually is inconvenient for the SOH estimation in practice. CNN has the characteristics of shared-weight architecture and translation invariance, which extracts the hierarchical feature and edge information on the data matrix automatically [51].

In summary, the SVM method has difficulty choosing the proper kernel function. RVM has a high demand for training data because of the sparse matrix. The process of adjusting hyper-parameters during training is cumbersome, because there are many hyper-parameters in GPR. The RNN method cannot be used for long-term estimation due to the vanishing gradients and exploding gradient problems. The robustness of LSTM is not strong, and the estimation accuracy of WNN is far less than that of deep networks. Extracting the data features manually is inconvenient in practice. Therefore, to address these problems and obtain a better prediction algorithm in this paper, a CNN–WNN–WLSTM is designed for SOH estimation. The proposed learning framework includes CNN layer and WNN–WLSTM layer, the CNN layer is used to extract the data features from the original battery data, and the WNN–WLSTM is adopted to produce the final SOH estimate by exploiting the features from the CNN. The WNN–WLSTM layer is made up of a fully connected layer and an LSTM layer whose activation function is replaced by the Morlet wavelet function. Thus, this model has both the advantages of WNN and LSTM, and it neither needs to select a proper kernel function nor adjust too many hyper-parameters. Finally, based on the battery data sets of NASA, the experiments are implemented to prove the performance of the suggested CNN–WNN–WLSTM algorithm. The experiments demonstrate that the estimations are superior to other existing GPR, BPNN, WNN, LSTM, WLSTM, and CNN–LSTM methods.

The contributions of this paper are as follows:

1. Based on WNN and LSTM, the neural network of WNN–WLSTM which just has two hidden layers is proposed. Compared with RNN and LSTM, the accuracy of the network estimation can be improved by adding only one hidden layer, which just add a small amount of complexity.
2. The method of CNN–WNN–WLSTM is developed to estimate the SOH. CNN is used to extract the spatial

**Fig. 1** Schematic structure of the CNN



features of battery raw data, and the designed WNN–WLSTM is then adopted to produce the final SOH estimation by exploiting the features from the CNN. The proposed method in this paper has higher estimation accuracy and faster convergence speed.

The remainder of this paper is organized as follows: the section "[Related works](#)" puts forward the definition of SOH, and the structure of CNN, LSTM, and WNN. In the section "[Proposed methods](#)", the proposed model of CNN–WNN–WLSTM is introduced. Then, the experiments and analysis are described in the section "[Experiments and discussion](#)". Finally, conclusions are given in the section "[Conclusion](#)".

## Related works

### SOH of battery

A common definition of SOH on cycle  $i$  is expressed as

$$\text{SOH}(i) = \frac{C_i}{C_0} \times 100\%, \quad (1)$$

where  $C_i$  denotes the measured capacity of cycle  $i$  and  $C_0$  denotes the original rated capacity.

In this paper, the SOH is computed by the capacity to estimate the state of the battery.

### Convolutional neural network

Figure 1 shows the schematic structure of the CNN that contains an input layer, a convolutional layer, a pooling layer, and a fully connected layer. The convolutional layer includes the weight and bias. The convolution kernels calculate the outputs using the dot product in the convolutional layer, and these outputs are called feature maps, which describe the features of the input data and then calculate non-linear by sigmoid activation function. The pooling layer is utilized to highlight features and lessen dimension that can prevent overfitting.

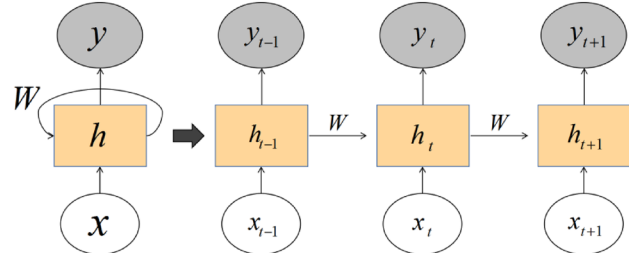


**Fig. 2** Schematic structure of the RNN

The input data are three-dimensional which includes width, height, and depth. The  $k$ th feature map is calculated by Eq. (2)

$$m_k = \sigma(W \cdot x_k + b_k), \quad (2)$$

where  $W$ ,  $b$ , and  $\sigma$  are the weight matrix, bias, and sigmoid activation function, respectively.

### Long short-term memory neural network

Unlike BPNN, RNN is a sort of neural network with a short-term memory function. Figure 2 shows the structure diagram of the RNN containing the hidden layer,  $h$ . This layer is unfolded in time steps  $t$ , and the sequence information of past steps propagating from  $h_{t-1}$  to  $h_t$  is saved by the hidden state. The output of this layer is exported at every step. However, because of the problems of vanishing gradients and exploding gradients, RNN cannot be used for long-term estimation.

To solve the above issues, LSTM is proposed, because it has a memory state, which can save the most important information. Figure 3 describes the structure of LSTM. It trains the network with a forget gate, input gate, output gate, and memory cells. This can be explained as follows:

$$f_t = \sigma(W_f \cdot [h_{t-1}, x_t] + b_f), \quad (3)$$

where  $x_t$  and  $x_t$  are the input status at the current time and the output state of the last hidden layer, respectively;  $W_f$ ,  $b_f$ , and  $f_t$  denote the weight, bias, and output of the forget gate, respectively;  $\sigma$  denotes the sigmoid activation function. The

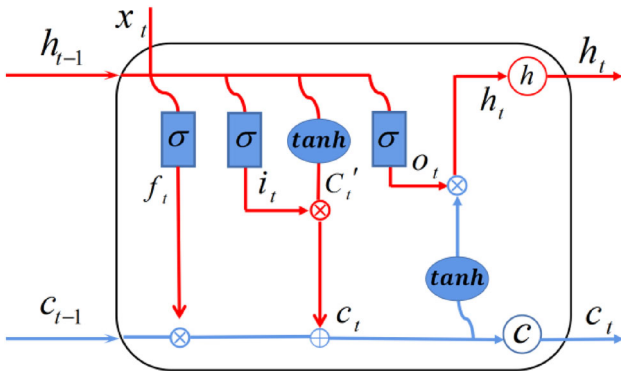


**Fig. 3** Schematic structure of the LSTM cell

output  $i_t$  in Fig. 3 is shown in Eq. (4)

$$i_t = \sigma(W_i \cdot [h_{t-1}, x_t] + b_i), \quad (4)$$

where  $W_i$ ,  $b_i$ , and  $i_t$  are the weight, bias, and output of the input gate, respectively.  $o_t$  in Fig. 3 is

$$o_t = \sigma(W_o \cdot [h_{t-1}, x_t] + b_o), \quad (5)$$

where the parameters  $W_o$ ,  $b_o$ , and  $o_t$  are the weight, bias, and output of the output gate, respectively. The third value  $C_t'$  is calculated by Eq. (6)

$$C_t' = \tanh(W_c \cdot [h_{t-1}, x_t] + b_c). \quad (6)$$

The variables  $W_c$ , and  $b_c$  are the weight and bias of the unit state, respectively.  $C_t'$  and  $\tanh$  are the state of the candidate cell and the activation function, respectively. Moreover,  $c_t$  is conducted from Eq. (7)

$$c_t = f_t \cdot c_{t-1} + i_t \cdot C_t'; \quad (7)$$

$c_{t-1}$ , and  $c_t$  are the states of the units at the previous and current times. Finally, the output  $h_t$  is obtained using Eq. (8)

$$h_t = o_t \cdot \tanh(c_t), \quad (8)$$

where  $h_t$  is the output of the hidden layer at the current time.

## Wavelet neural network

The WNN can adaptively produce the parameters of wavelet templates [52]. Compared with normally used neural networks such as BPNN, the activation function is substituted by a group of wavelet functions that are generated from the Morlet wavelet generating function [39].

The schematic structure of WNN, which includes three layers, is shown in Fig. 4. It contains  $K$  nodes in the input layer,  $L$  nodes in the hidden layer, and  $K$  nodes in the output

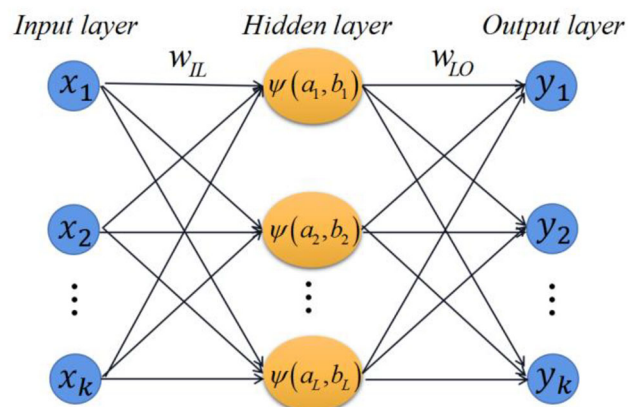


**Fig. 4** Schematic structure of the WNN

layer. The parameters in the hidden layer, which are continually regulated during the learning process, are made up of the weights  $w_{il}$ ,  $w_{lo}$ , the wavelet dilation parameter  $a$ , and the wavelet translation parameter  $b$ . The  $y_i$  of the output layer is related to the input data  $x_i$ . It can be illustrated as follows:

$$net_l = \frac{w_{il}x_i - b_l}{a_l} \quad (l = 1, 2, \dots, L) \quad (9)$$

$$x_l = \psi_{a_l, b_l}(net_l) \quad (l = 1, 2, \dots, L) \quad (10)$$

$$y_i = \sum_{l=1}^{l=L} w_{lo}x_l \quad (i = 1, 2, \dots, k). \quad (11)$$

$\psi(x)$  is the generating function, which is defined as the Morlet wavelet function, and is widely used as an activation function in neural networks

$$\psi(x) = \cos(1.75x) \exp(-0.5x^2). \quad (12)$$

## Proposed methods

### WNN–WLSTM structure

To further perfect the estimation accuracy of the network, this paper proposes the two hidden layer WNN–WLSTM, which is based on the LSTM and WNN neural networks. This model has the advantages of both rapid convergence of the WNN and saving the vital data information of LSTM. The structure of the WNN–WLSTM is shown in Fig. 5.

Compared with the WNN structure shown in Fig. 4, the WNN–WLSTM adds another hidden layer of the WLSTM after the WNN units. As Fig. 5 shows, there are four layers in the new structure: input layer, hidden layer one, i.e., the WNN layer, hidden layer two, i.e., the WLSTM layer, and output

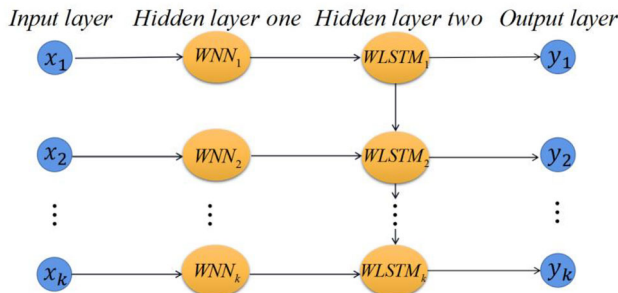


**Fig. 5** Schematic structure of the WNN–WLSTM

layer. The output of hidden layer one is labeled  $x_l$ , which is related to the input data  $x_i$ . They have been explained in Eqs. (9) and (10).

Compared with the normal fully connected layer,  $x_l$  is the hypothetical input data of hidden layer two, which is approximated by linear superposition of wavelet basis functions by the fully connected hidden layer one.

Hidden layer two is the WLSTM layer, and the activation functions in LSTM are replaced by the Morlet wavelet function; thus, Eqs. (3–6) and (8) are reformulated as

$$f_t = M(W_f \cdot [h_{t-1}, x_t] + b_f) \quad (13)$$

$$i_t = M(W_i \cdot [h_{t-1}, x_t] + b_i) \quad (14)$$

$$o_t = M(W_o \cdot [h_{t-1}, x_t] + b_o) \quad (15)$$

$$C_t' = M(W_c \cdot [h_{t-1}, x_t] + b_c) \quad (16)$$

$$h_t = o_t \cdot M(c_t). \quad (17)$$

$M$  in Eqs. (13–17) is denoted as the Morlet wavelet function. For Eq. (7), because there is no activation function, the WLSTM still adopts the original formula.

The adjusted WLSTM layer can also extract the time series features of battery data. Experimental results demonstrate that the modified LSTM has a more accurate estimation performance.

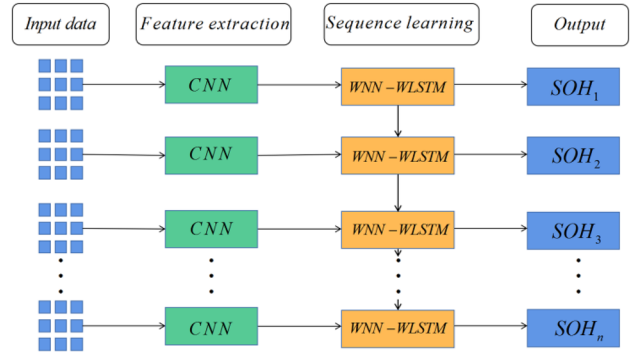


**Fig. 6** Structure of SOH estimation method based on CNN–WNN–WLSTM

### CNN–WNN–WLSTM structure

To extract the data features more easily, CNN is designed before WNN–WLSTM. Compared with manually extraction for input data features [50], this CNN structure can extract the data features automatically. The detailed structure of CNN–WNN–WLSTM is shown in Fig. 6.

The loss function quantifying the discrepancy between the model's predicted and measured numerical values is formulated by Eq. (18)

$$L = \frac{1}{K} \sum_{i=1}^K (y_i - y_i^*)^2; \quad (18)$$

herein,  $K$ ,  $y_i$ , and  $y_i^*$  are the total data cycles, the actual SOH, and predicted SOH in the step of  $t$ , respectively.

The minimized loss function is determined by the optimizer. This paper chooses RMSprop as the optimizer, which can speed up the network training speed and further achieve global optimization.

### CNN–WNN–WLSTM-based SOH estimation algorithm

In this section, the framework of SOH estimation method based on CNN–WNN–WLSTM is demonstrated in Fig. 7, this model includes CNN layer, WNN layer and WLSTM layer, and they are connected by the fully connected layer. “Cov2D” and ReLU denote the two-dimensional convolution and ReLU activation function. The presented CNN–WNN–WLSTM-based SOH estimation is described in Algorithm 1.

**Algorithm 1** CNN–WNN–WLSTM-based SOH estimation

---

**Input:** The set of SOH measurements  $\{x_i, y_i\}_{i=1}^N$  is used for training, where  $x_i$  and  $y_i$  are the data matrix and the SOH at the  $i$ -th cycle.

**Output:** SOH estimation results  $\{\hat{y}_j\}_{j=1}^K$ , which correspond to all cycles of the battery in the whole process or the partial cycles.

**Training:**

1. Initialize the network parameters: the wavelet dilation parameter  $a$ , the wavelet translation parameter  $b$ , the biases, and the weights of all layers to layers in CNN–WNN–WLSTM.
2. The CNN layer is used to process the input data, and form a spatial feature  $\{m_{k_i}\}_{i=1}^R$  to WNN layer.
3. The WNN layer is utilized to form a data feature  $\{x_{l_i}\}_{i=1}^M$  to WLSTM layer, which is approximated by linear superposition of wavelet basis functions and can be evaluated by Eqs. (9) and (10).
4. The time series feature of the data  $\{h_{t_i}\}_{i=1}^L$  are extracted by the WLSTM layer.
5. Calculate the error between the estimated value  $\{\hat{y}_i\}_{i=1}^N$  and the real value  $\{y_i\}_{i=1}^N$  by using the loss function (18).
6. The RMSprop optimization algorithm and gradient descent method are utilized to optimize the wavelet dilation parameter  $a$ , the wavelet translation parameter  $b$ , and the weights of all layers to layers in CNN–WNN–WLSTM.

**Testing:**

7. Set the estimation steps  $m$ .
  8. The testing data  $\{x_j\}_{j=1}^K$  and the trained models are used to estimate and obtain the estimated SOH value  $\{\hat{y}_j\}_{j=1}^K$ .
- 

The specifications of the CNN–WNN–WLSTM architecture is shown in Table 1. For the numbers of input and output data in Algorithm 1,  $N$  equals 336 and  $K$  equals 168 in the section "Estimation and comparison I", while in the section

"Estimation and comparison II",  $N$  equals 436 and  $K$  equals 68. The network parameters of the wavelet dilation parameter  $a$ , the wavelet translation parameter  $b$ , the biases, and the weights of all layers to layers in CNN–WNN–WLSTM are

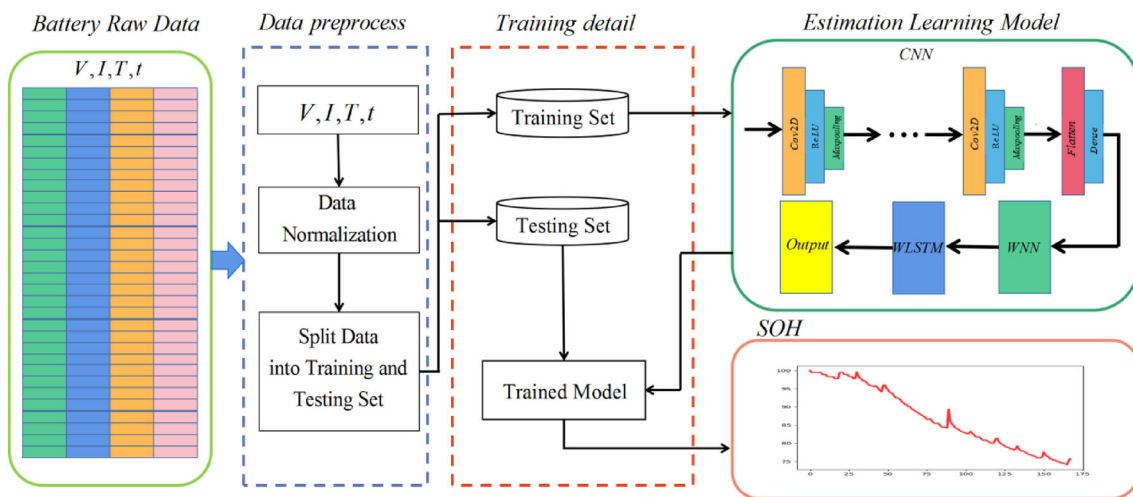


**Fig. 7** The framework of SOH estimation method based on CNN–WNN–WLSTM

**Table 1** Parameter settings of the CNN–WNN–WLSTM architecture

Layer	Input shape	Kernel size	Kernel number	Output shape	Last/next layer
I0	$784 \times 4$	N/A	N/A	$784 \times 4$	N/A/C1
C1	$784 \times 4$	$3 \times 3$	64	$64 \times 784 \times 4$	I0/P1
P1	$64 \times 784 \times 4$	$2 \times 2$	N/A	$64 \times 783 \times 3$	C1/C2
C2	$64 \times 783 \times 3$	$3 \times 3$	64	$64 \times 783 \times 3$	P1/P2
P2	$64 \times 783 \times 3$	$2 \times 2$	N/A	$64 \times 782 \times 2$	C2/C3
C3	$64 \times 782 \times 2$	$1 \times 1$	64	$64 \times 782 \times 2$	P2/P3
P3	$64 \times 782 \times 2$	$2 \times 2$	N/A	$64 \times 391 \times 1$	C3/F1
F1	$64 \times 391 \times 1$	N/A	N/A	$1 \times 25,024$	P3/D1
D1	$1 \times 25,024$	N/A	64	$1 \times 64$	F1/WNN1
WNN1	$1 \times 64$	N/A	60	$1 \times 60$	D1/WLSTM1
WLSTM1	$1 \times 60$	N/A	100	$1 \times 100$	WNN1/O0
O0	$1 \times 100$	N/A	1	1	WLSTM1/N/A

I input layer, C convolutional layer, P maxpooling layer, F flatten layer, D dense layer, WNN WNN layer, WLSTM WLSTM layer, O output layer

randomly initialized by Python 3.8. The numbers of features  $R$  in Step 2 equal 64,  $M$  in Step 3 equal 60, and  $L$  in Step 4 equal 100 in CNN–WNN–WLSTM.

## Experiments and discussion

### Experimental environment

Experimental hardware facilities use Inter(R) Core(TM) i5-7200u CPU @ 2.50GHZ processor, Windows7 flagship edition 64-bit operating system, and 8 GB running memory. The programming software is Python 3.8, and the deep learning framework Keras is used to support the construction of the CNN–WNN–WLSTM neural network simulation model, which is based on TensorFlow.

### Data sets

To comprehensively discuss the performance of the proposed method, in this paper, the cyclic aging data of lithium-ion batteries are chosen from the NASA Ames PCoE [53].

The data set of the NASA Ames PCoE includes 36 Li-ion battery data: No. 5, No. 6, No. 7, No. 18, and No. 25–56. Because these 36 batteries are different in the lengths of the SOHs, the No. 5, No. 6, and No. 7 batteries are the most widely utilized in related papers, because they are much longer and have the same length [54].

In this paper, the data sets from these three batteries are produced using Eq. (1) to carry out the experiments, which consist of training and testing processes. The SOH attenuation curve tracks of the three batteries are displayed in Fig. 8. The total charge and discharge cycles of each battery are 168.

It is noteworthy that the SOH does not appear to be the law in a humdrum declining manner with the cycle number, but an evident overall degradation trend and local regeneration phenomenon.

## Data explanation and preprocessing

### Data explanation

The three subfigures in Fig. 9 are the charging curves of voltage, current, and temperature of the No. 5 battery at different cycle numbers. With the increase in the cycle numbers, the time cost of CC charging, and reaching the cut-off voltage of the battery is shortened; moreover, the peak temperature of charging curves is increasing, and the time of reaching the peak temperature is advancing, which are the aging process of batteries. In addition, the variation ranges of current, voltage, and temperature are 1500–4500 times, 0–3500 times, and 2000–4500 times, respectively. To fully extract these three aging characteristics, this paper chooses the data from the entire CC charge and fragment CV charge, that is, the first 5000 times [55]. Then, the fusion features composed of aging factors, such as current, voltage, and temperature, are extracted by CNN.

### Data preprocessing

Based on the aging factors of battery, the input data are formulated as follows:

$$x^j = \begin{vmatrix} V_1 & I_1 & T_1 & t_1 \\ V_2 & I_2 & T_2 & t_2 \\ \vdots & \vdots & \vdots & \vdots \\ V_i & I_i & T_i & t_i \end{vmatrix}; \quad (19)$$

$x^j$  denotes the input of the  $j$ th cycle.  $V_i$ ,  $I_i$ ,  $T_i$ , and  $t_i$  are the charging voltage, current, temperature, and time in the original battery data, respectively.

The range of each column in the input data is inconsistent, which will lead to poor network training effect. Thus, the input data are normalized firstly via Eq. (20)

$$x_{norm} = \frac{x_i - x_{\min}}{x_{\max} - x_{\min}}, \quad (20)$$

where  $x_i$ ,  $x_{\min}$ , and  $x_{\max}$  are the original value, and minimum and maximum values of  $x$ .

### Evaluation metrics

To intuitively compare the performance of the estimation methods, two evaluation metrics of root-mean-square error

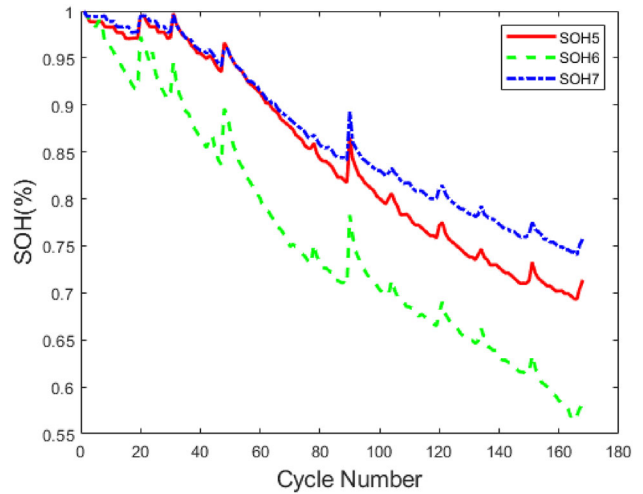


**Fig. 8** The SOH degradation curves of batteries No. 5, No. 6, and No. 7

(RMSE) and the mean absolute percentage error (MAPE) are presented in this paper, which are formulated as follows:

$$RMSE = \sqrt{\frac{\sum_{i=1}^m (y_i - \hat{y}_i)^2}{m}} \quad (21)$$

$$MAPE = \frac{1}{m} \sum_{i=1}^m \left| \frac{y_i - \hat{y}_i}{y_i} \right|, \quad (22)$$

where  $m$ ,  $y_i$ , and  $\hat{y}_i$  are the estimation steps, the actual SOH, and the predicted SOH, respectively.

### Optimizer comparison

To verify that the RMSprop optimizer can speed up the network training speed and further achieve global optimization, the Adagrad optimizer is chosen as a control group. The CNN–WNN–WLSTM method is used to perform this experiment. Figure 10 and Table 2 are the estimation results of two optimizers for battery No. 5. It can be seen that the line of RMSprop is closer to the red line when using the RMSprop optimizer. Figure 11 shows that RMSprop can achieve faster convergence and further global optimization than Adagrad.

### Estimation and comparison I

#### Data set organization

In this part, the data settings are shown in Fig. 12. The training data from any two of the batteries are utilized for training the proposed CNN–WNN–WLSTM model, and the remaining battery is used for estimation.

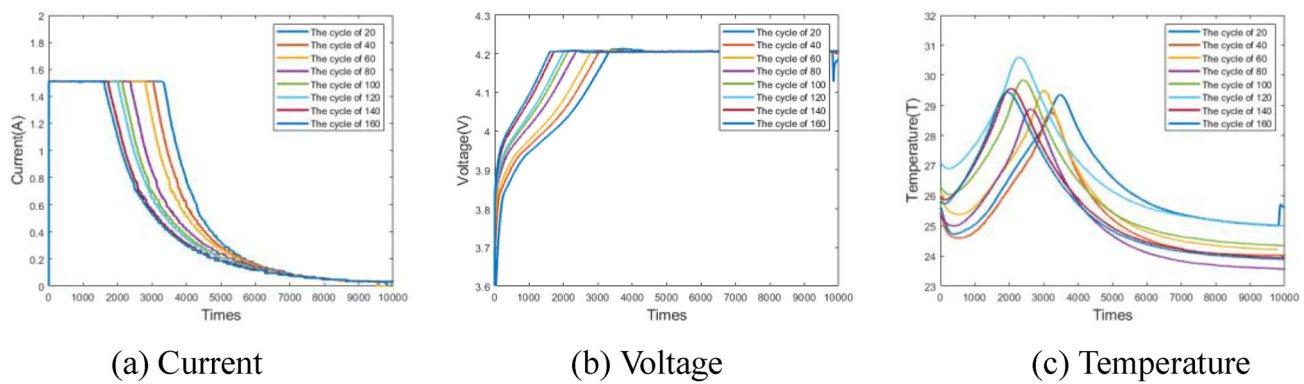


**Fig. 9** Three charging curves of the No. 5 battery at different cycle numbers

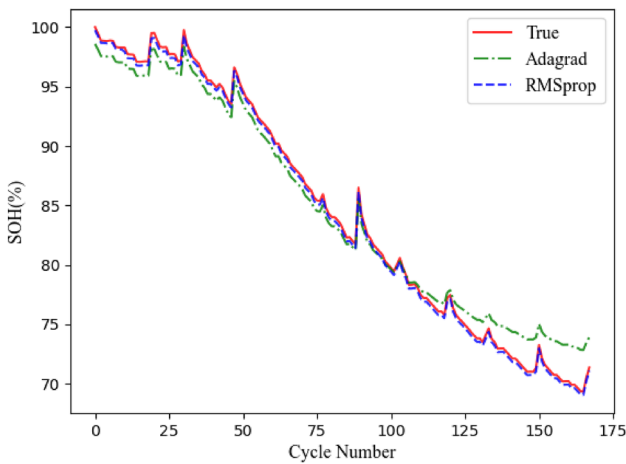


**Fig. 10** Estimation results of the two optimizers for battery No. 5

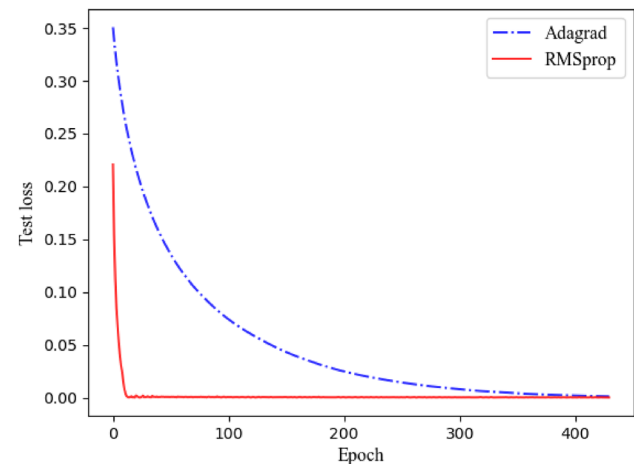


**Fig. 11** The test loss value change with the epochs under CNN–WNN–WLSTM

**Table 2** Estimation error comparison of the two optimizers for battery No. 5

No. 5	Adagrad	RMSprop
RMSE	0.014918	0.005744
MAPE	0.015840	0.006860

#### Estimation for the whole process

In this part, the proposed CNN–WNN–WLSTM model is compared with the following methods:

**BPNN** [34]: The algorithm is momentum BP (MOBP) and has three layers. While BPNN in this paper do not adopt momentum, it is just a three-layer fully connected back-propagation neural network.

**WNN** [39]: a three-layer fully connected neural network in which the hidden layer is improved by the wavelet dilation parameter and the wavelet translation parameter; its structure is shown in Fig. 4.

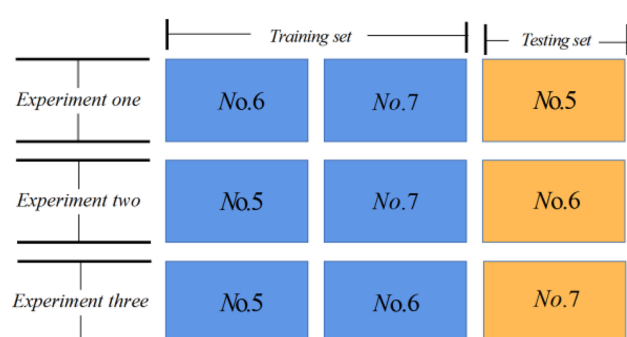


**Fig. 12** Organization of the training and testing sets for three experiments

**LSTM** [43]: a three-layer LSTM neural network. The schematic structure of LSTM can be seen in Fig. 3.

**WLSTM**: a three-layer WLSTM neural network, and the introduction of WLSTM can be seen in the section "WNN–WLSTM structure".

**CNN–LSTM** [56]: a deep learning neural network composed of CNN and LSTM.

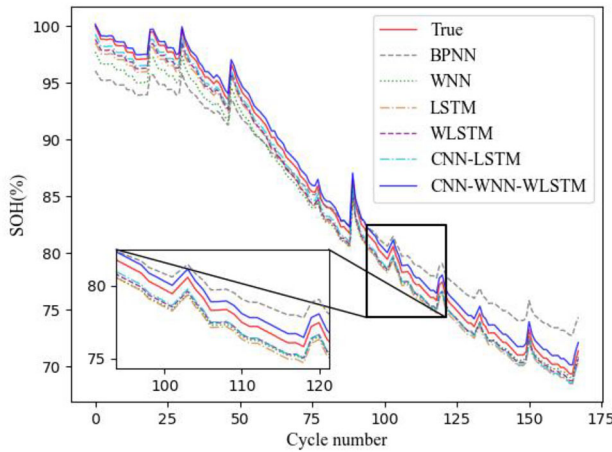


**Fig. 13** Estimation results of the six models for battery No. 5

The input data of BPNN, WNN, LSTM, and WLSTM are the time cost of CC charging.

The estimation results of six models, BPNN, WNN, LSTM, WLSTM, CNN-LSTM, and CNN-WNN-WLSTM, for the three batteries are shown in Figs. 13, 15 and 17, respectively. As depicted in Fig. 13, the red line indicates the measured SOH, and the other dotted lines refer to the estimated SOH result. Taking Fig. 13 as an example, the estimation result of the BPNN is not well. For the WNN model, there is a significant distance between the estimated value and the measured value in the period of 1 to 50 cycles, which means that the WNN method is not suitable in predicting the SOH of No. 5. LSTM is better than the method of WNN, but it still does not perform well in the cycles from 1 to 25. The WLSTM is slightly better than the LSTM model. Because the input of CNN-LSTM is integrated into the three aging characteristics of battery, so it is better than WLSTM. The simulation of the experiment with the CNN-WNN-WLSTM model is shown as the blue line. Compared to the other dotted lines, it is clear that the blue line is the closest to the red line, which means that the proposed method has the strongest predictive performance of the five methods.

Figures 14 shows the estimation errors of six models for battery No. 5; compared with other method, CNN-WNN-WLSTM has a smallest SOH error. The estimation error comparison of the six models for battery No. 5 is shown in Table 3, which shows that the prognostic RMSEs of BPNN, WNN, LSTM, WLSTM, and CNN-LSTM are 2.4987%, 1.4761%, 1.1147%, 0.8608%, and 0.7231%, respectively, but the RMSE of the CNN-WNN-WLSTM is 0.5744%. Similarly, the Mapes of BPNN, WNN, LSTM, WLSTM, and CNN-LSTM are 2.6688%, 1.3443%, 1.3188%, 1.0060%, and 0.8712%, respectively, while the MAPE of the proposed method is 0.6860%. These values mean that the CNN-WNN-WLSTM model has a best predictive ability compared to the BPNN, WNN, LSTM, WLSTM, and CNN-LSTM.

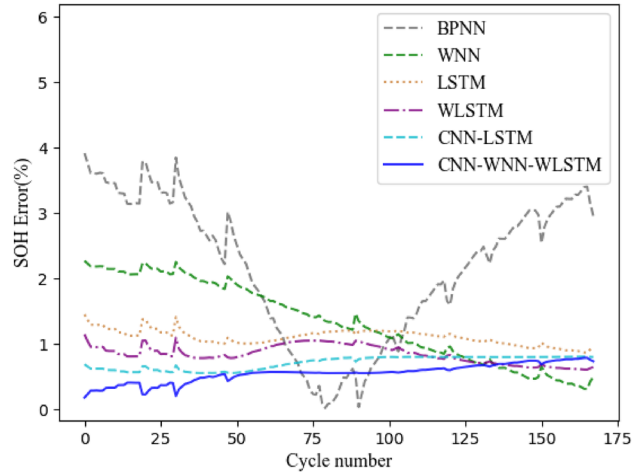


**Fig. 14** Estimation errors of the six models for battery No. 5

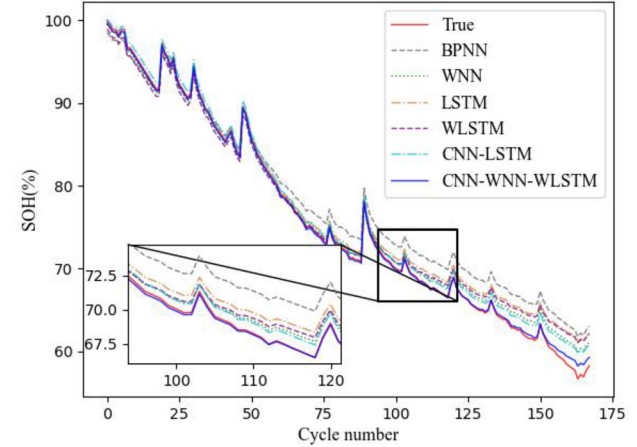


**Fig. 15** Estimation results of the six methods for battery No. 6

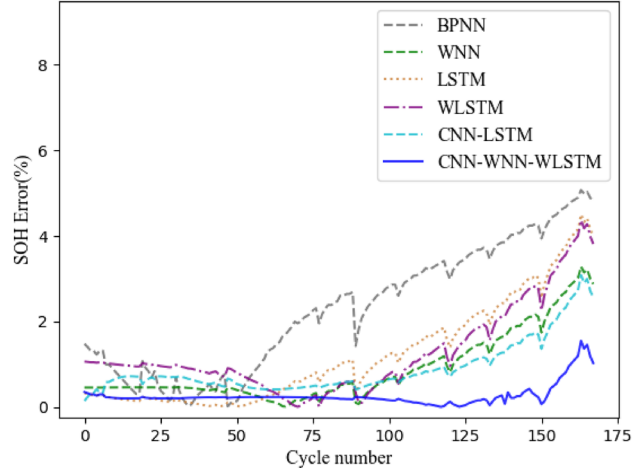


**Fig. 16** Estimation errors of the six models for battery No. 6

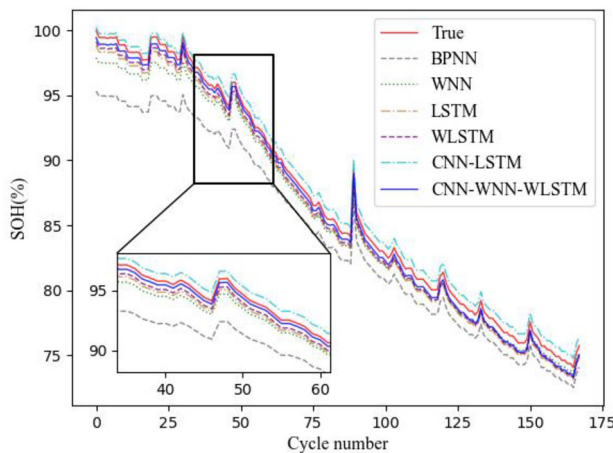


**Fig. 17** Estimation results of the six methods for battery No. 7

The results of the estimation for the remaining two batteries are similar to those of No. 5. The estimations of the six neural network models for them are depicted in Figs. 15 and 17, and the SOH errors are shown in Figs. 16 and 18, and the estimation error comparisons are shown in Tables 4 and 5.

By comparing Figs. 13, 14, 15, 16, 17 and 18 and Tables 3, 4 and 5, three conclusions can be obtained:

1. The error of LSTM is usually smaller than that of WNN in predicting the SOH values of batteries No. 5 and No. 7, but WNN is better than LSTM in predicting the SOH values of battery No. 6. As shown in Fig. 8, the SOH curves of No. 5 and No. 7 have the similar local regeneration phenomenon changes; thus, the memory unit will learn these changes and further obtain more accurate SOH estimation performance for No. 5 or No. 7 batteries during LSTM training. However, the SOH curve of No. 6 varies greatly and is different from those of No. 5 and No. 7, so

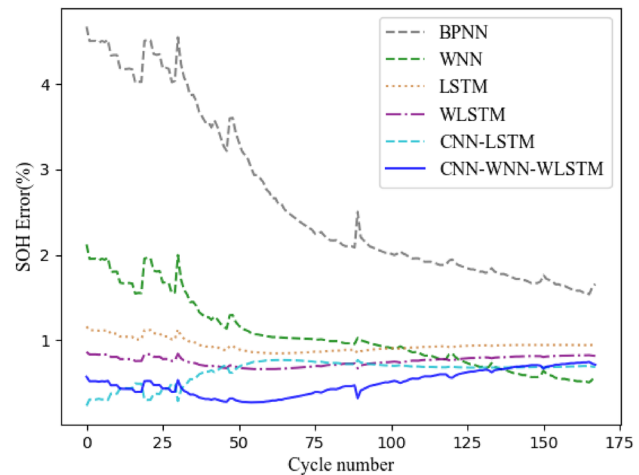


**Fig. 18** Estimation errors of the six models for battery No. 7

the estimation performance of the LSTM method is not ideal. This phenomenon also occurs for WLSTM.

2. When the WNN method is used for predicting the SOH values of three batteries, its results are more stable than LSTM, and the range of RMSEs and Mapes of this method is no more than 2%. This is because this network has the ability to automatically adjust wavelet parameters, so its robustness is better than LSTM.
3. Because the CNN-WNN-WLSTM method is combining the advantages of LSTM and WNN and using CNN to process the three aging factors of battery, thus, the RMSE and MAPE are smaller than WNN, WLSTM and CNN-LSTM in predicting the SOH values of the No. 5, No. 6, and No. 7 batteries.

**Table 3** Estimation errors comparison of the six models for battery No. 5

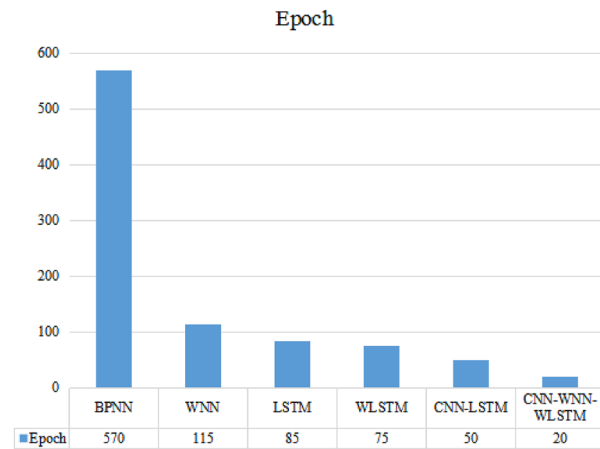
No. 5	BPNN	WNN	LSTM	WLSTM	CNN-LSTM	CNN-WNN-WLSTM
RMSE	0.024987	0.014761	0.011147	0.008608	0.007231	0.005744
MAPE	0.026688	0.013443	0.013188	0.010060	0.008712	0.006860

**Table 4** Estimation errors' comparison of the six models for battery No. 6

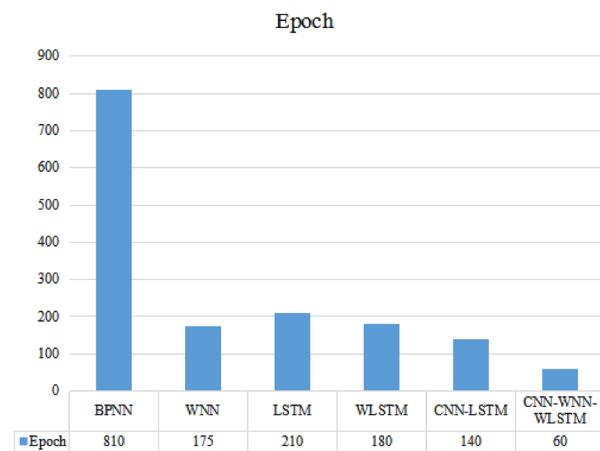
No. 6	BPNN	WNN	LSTM	WLSTM	CNN-LSTM	CNN-WNN-WLSTM
RMSE	0.028211	0.016632	0.022945	0.019838	0.010724	0.008006
MAPE	0.035583	0.019512	0.026720	0.021053	0.012890	0.009157

**Table 5** Estimation errors' comparison of the six models for battery No. 7

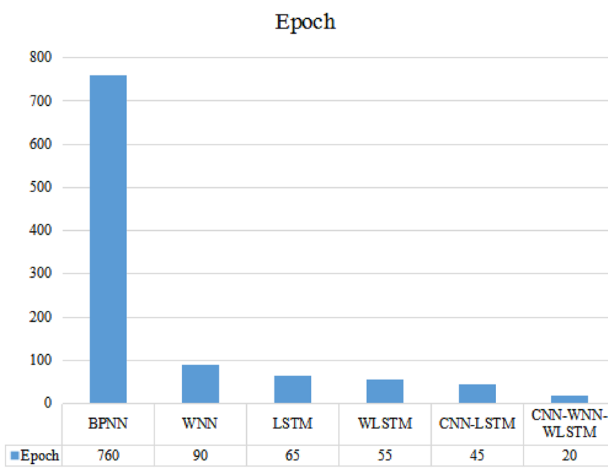
No. 7	BPNN	WNN	LSTM	WLSTM	CNN-LSTM	CNN-WNN-WLSTM
RMSE	0.029074	0.011439	0.009445	0.007588	0.006511	0.005173
MAPE	0.028644	0.011900	0.010898	0.008806	0.007486	0.005895



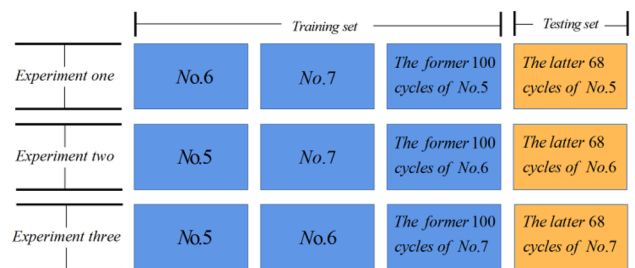
(a) Epoch cost for battery No. 5



(b) Epoch cost for battery No. 6



(c) Epoch cost for battery No. 7

**Fig. 19** Epoch cost (numbers) of all neural networks for the three batteries**Fig. 20** Organization of the training and testing sets for three experiments

### Epoch cost

To illustrate the advantage of the fast convergence of CNN–WNN–WLSTM, the epoch costs of these six neural networks when the accuracy of test loss reached 0.01 are shown in Fig. 19.

As seen from the above three subfigures, CNN–WN–WLSTM uses the most minor epochs when meeting the given accuracy requirements, which means that the proposed method can extract and store important information effectively, it enables CNN–WNN–WLSTM to meet the accuracy requirements without more repeated training.

## Estimation and comparison II

### Data set organization

In this part, the data settings are shown in Fig. 20. The training data from any two of the batteries and the partial cycles of the three batteries (the former 100 cycles) are used for training the proposed CNN–WNN–WLSTM model, and the remaining cycles of the three batteries (the latter 68 cycles) are used for estimation.

### Estimation for the partial process

To further demonstrate the predictive power of the presented method, a comparison experiment for partial battery data with the GPR-based methods proposed by Zhou et al. is implemented [57]. GPR is the basic Gaussian process regression method, while the other three models with neural network functions as kernels are shown as Model I, Model II, and Model III: the neural network itself, the sum of the neural network, and the Maternard covariance function and the product of the neural network and the periodic covariance function. These methods only predict the last 68 SOH values for No. 5, No. 6, and No. 7. Figures 21, 22 and 23 show the estimation results of CNN–WNN–WLSTM, and Tables 6, 7 and 8 show the estimation errors of basic GPR, three optimized GPR, and CNN–WNN–WLSTM. The comparison

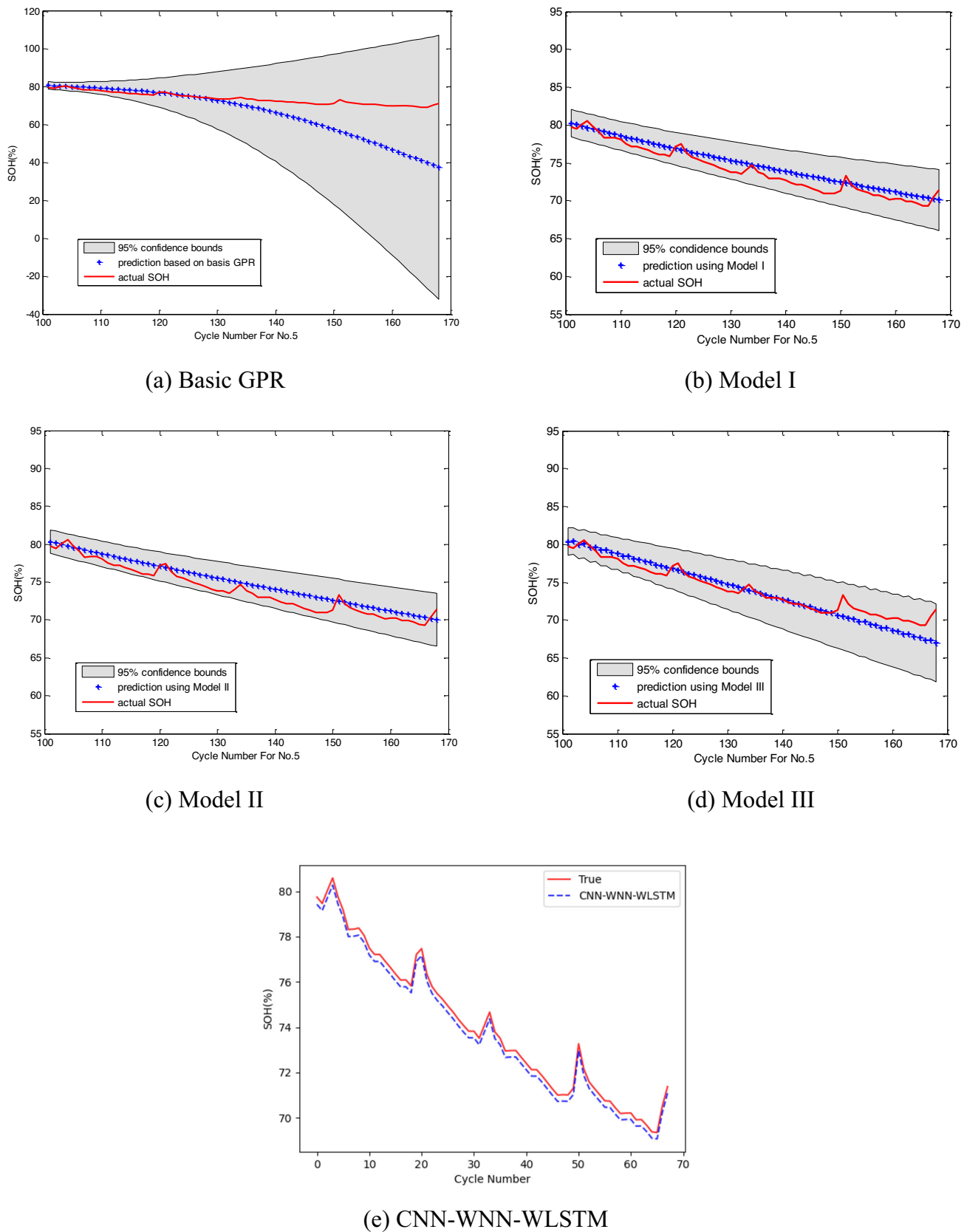
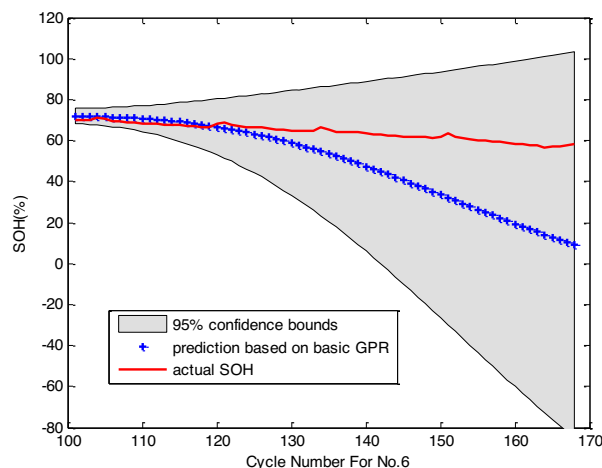
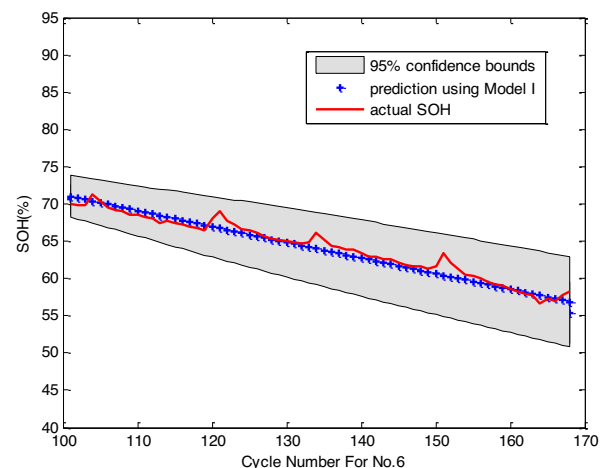


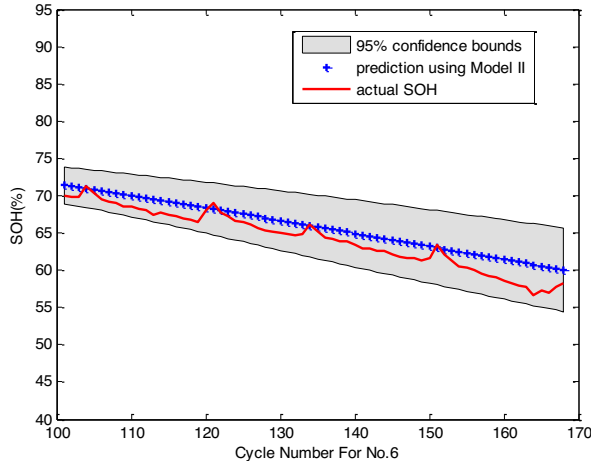
**Fig. 21** Estimation results of four GPR models and CNN–WNN–WLSTM for battery No. 5



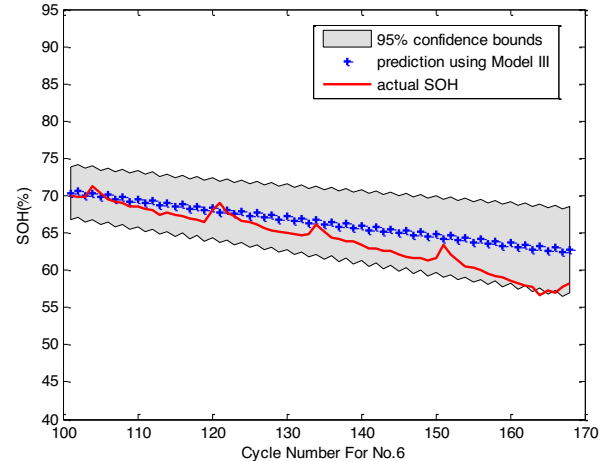
(a) Basic GPR



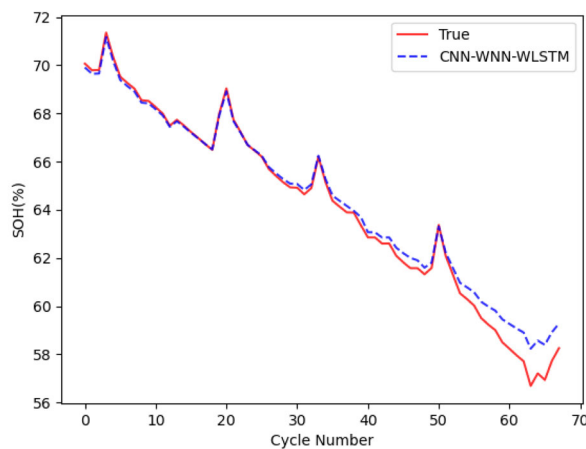
(b) Model I



(c) Model II



(d) Model III



(e) CNN-WNN-WLSTM

**Fig. 22** Estimation results of four GPR models and CNN–WNN–WLSTM for battery No. 6

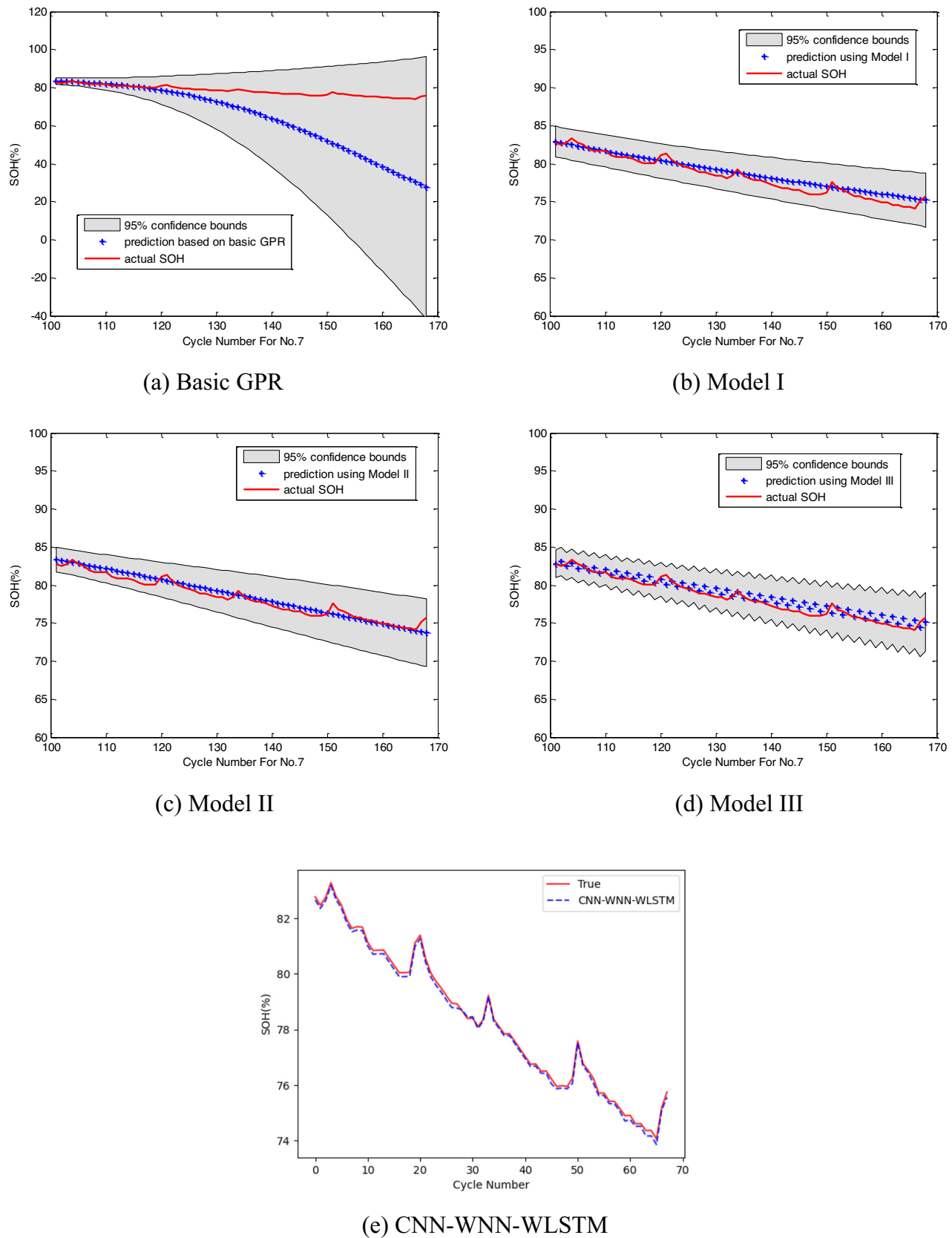


**Fig. 23** Estimation results of four GPR models and CNN–WNN–WLSTM for battery No. 7

**Table 6** Estimation errors' comparison of four GPR models and CNN–WNN–WLSTM for battery No. 5

No. 5	GPR	Model I	Model II	Model III	CNN–WNN–WLSTM
RMSE	0.1303	0.0074	0.0083	0.0083	0.0027
MAPE	0.1213	0.0080	0.0094	0.0091	0.0036

**Table 7** Estimation errors' comparison of four GPR models and CNN–WNN–WLSTM for battery No. 6

No. 6	GPR	Model I	Model II	Model III	CNN–WNN–WLSTM
RMSE	0.2251	0.0082	0.0081	0.0171	0.0039
MAPE	0.2699	0.0100	0.0099	0.0218	0.0053

**Table 8** Estimation errors' comparison of four GPR models and CNN–WNN–WLSTM for battery No. 7

No. 7	GPR	Model I	Model II	Model III	CNN–WNN–WLSTM
RMSE	0.2074	0.0066	0.0068	0.0099	0.0021
MAPE	0.1918	0.0074	0.0073	0.0112	0.0025

results indicate that CNN–WNN–WLSTM can obtain better estimation accuracy. In particular, the proposed method has better estimation performances for the local regeneration phenomenon existing in the real SOH curves; however, the GPR-based estimation methods could not indicate these local features.

## Conclusion

In this paper, a novel estimation model of battery SOH based on CNN, WNN, and WLSTM is presented. To further improve the estimation accuracy, an improved network structure named CNN–WNN–WLSTM is designed for battery health monitoring; both have the advantages of rapid convergence and extracts the data features of the input data automatically. Compared with other popular neural network methods, the proposed method has a lowest estimation error. Experimental results for the entire battery cycle and partial battery cycle both confirm that this proposed method has high estimation accuracy for lithium-ion batteries with even complicated phenomena. Exploring SOH estimation methods, especially for real-time estimation with better performance, will be the future work.

**Acknowledgements** This work is supported by the Heilongjiang Provincial Natural Science Foundation (CN) (LH2022F032) and the Shandong Provincial Natural Science Foundation (CN) (ZR2022LLZ003).

**Data availability** All relevant data are within the paper.

## Declarations

**Conflict of interest** The authors have no relevant financial or non-financial interests to disclose.

**Open Access** This article is licensed under a Creative Commons Attribution 4.0 International License, which permits use, sharing, adaptation, distribution and reproduction in any medium or format, as long as you give appropriate credit to the original author(s) and the source, provide a link to the Creative Commons licence, and indicate if changes were made. The images or other third party material in this article are included in the article's Creative Commons licence, unless indicated otherwise in a credit line to the material. If material is not included in the article's Creative Commons licence and your intended use is not permitted by statutory regulation or exceeds the permitted use, you will need to obtain permission directly from the copyright holder. To view a copy of this licence, visit <http://creativecommons.org/licenses/by/4.0/>.

## References

- Kim ILS (2009) A technique for estimating the state of health of lithium batteries through a dual-sliding-mode observer. *IEEE Trans Power Electron* 25(4):1013–1022
- Nishi Y (2001) Lithium ion secondary batteries; past 10 years and the future. *J Power Sources* 100(1–2):101–106
- Blomgren GE (2016) The development and future of lithium ion batteries. *J Electrochem Soc* 164(1):A5019
- Chombo PV, Lagoonual Y (2020) A review of safety strategies of a Li-ion battery. *J Power Sources* 478:228649
- Zhang J, Lee J (2011) A review on prognostics and health monitoring of Li-ion battery. *J Power Sources* 196(15):6007–6014
- Wang Y, Tian J, Sun Z et al (2020) A comprehensive review of battery modeling and state estimation approaches for advanced battery management systems. *Renew Sustain Energy Rev* 131:110015
- Saha B, Poll S, Goebel K et al (2007) An integrated approach to battery health monitoring using Bayesian regression and state estimation. In: 2007 IEEE Autotestcon. IEEE, pp 646–653
- Vichard L, Ravey A, Venet P et al (2021) A method to estimate battery SOH indicators based on vehicle operating data only. *Energy* 225:120235
- Zhou W, Zheng Y, Pan Z et al (2021) Review on the battery model and SOC estimation method. *Processes* 9(9):1685
- Shu X, Li G, Shen J et al (2020) An adaptive fusion estimation algorithm for state of charge of lithium-ion batteries considering wide operating temperature and degradation. *J Power Sources* 462:228132

11. Ji Y, Chen Z, Shen Y et al (2021) An RUL prediction approach for lithium-ion battery based on SADE-MESN. *Appl Soft Comput* 104:107195
12. Cai L, Meng J, Stroe DI et al (2020) Multiobjective optimization of data-driven model for lithium-ion battery SOH estimation with short-term feature. *IEEE Trans Power Electron* 35(11):11855–11864
13. Saha B, Goebel K, Poll S et al (2008) Prognostics methods for battery health monitoring using a Bayesian framework. *IEEE Trans Instrum Meas* 58(2):291–296
14. Shu X, Li G, Zhang Y et al (2020) Online diagnosis of state of health for lithium-ion batteries based on short-term charging profiles. *J Power Source* 471:228478
15. Olivares BE, Munoz MAC, Orchard ME et al (2012) Particle-filtering-based prognosis framework for energy storage devices with a statistical characterization of state-of-health regeneration phenomena. *IEEE Trans Instrum Meas* 62(2):364–376
16. Chen Z, Xue Q, Xiao R et al (2019) State of health estimation for lithium-ion batteries based on fusion of autoregressive moving average model and Elman neural network. *IEEE Access* 7:102662–102678
17. Lyu C, Zhang T, Luo W et al (2019) SOH estimation of lithium-ion batteries based on fast time domain impedance spectroscopy. In: 2019 14th IEEE conference on industrial electronics and applications (ICIEA). IEEE, pp 2142–2147
18. Kwiecien M, Badeda J, Huck M et al (2018) Determination of SoH of lead-acid batteries by electrochemical impedance spectroscopy. *Appl Sci* 8(6):873
19. Liu Y, Wang L, Li D et al (2023) State-of-health estimation of lithium-ion batteries based on electrochemical impedance spectroscopy: a review. *Prot Control Mod Power Syst* 8(1):1–17. <https://doi.org/10.1186/s41601-023-00314-w>
20. Birk CR, Roberts MR, McTurk E et al (2017) Degradation diagnostics for lithium ion cells. *J Power Sources* 341:373–386
21. Zhang J, Wang P, Gong Q et al (2021) SOH estimation of lithium-ion batteries based on least squares support vector machine error compensation model. *J Power Electron* 21(11):1712–1723
22. Li L, Cui W, Hu X et al (2021) A state-of-health estimation method of lithium-ion batteries using ICA and SVM. In: 2021 global reliability and prognostics and health management (PHM-Nanjing). IEEE, pp 1–5
23. Lyu Z, Wang G, Gao R (2022) Synchronous state of health estimation and remaining useful lifetime prediction of Li-ion battery through optimized relevance vector machine framework. *Energy* 251:123852
24. Wang S, Zhang X, Chen W et al (2021) State of health prediction based on multi-kernel relevance vector machine and whale optimization algorithm for lithium-ion battery. *Trans Inst Meas Control* 1–13
25. Zheng X, Deng X (2019) State-of-health prediction for lithium-ion batteries with multiple Gaussian process regression model. *IEEE Access* 7:150383–150394
26. Qu J, Liu F, Ma Y et al (2019) A neural-network-based method for RUL prediction and SOH monitoring of lithium-ion battery. *IEEE Access* 7:87178–87191
27. Ma P, Cui S, Chen M et al (2023) Review of family-level short-term load forecasting and its application in household energy management system. *Energies* 16(15):5809. <https://doi.org/10.3390/en16155809>
28. Shu X, Shen S, Shen J et al (2021) State of health prediction of lithium-ion batteries based on machine learning: advances and perspectives. *Iscience* 24(11):103265
29. Kaur K, Garg A, Cui X et al (2021) Deep learning networks for capacity estimation for monitoring SOH of Li-ion batteries for electric vehicles. *Int J Energy Res* 45(2):3113–3128
30. Fan Y, Xiao F, Li C et al (2020) A novel deep learning framework for state of health estimation of lithium-ion battery. *J Energy Storage* 32:101741
31. Bonfitto A (2020) A method for the combined estimation of battery state of charge and state of health based on artificial neural networks. *Energies* 13(10):2548
32. Bonfitto A, Ezemobi E, Amati N et al (2019) State of health estimation of lithium batteries for automotive applications with artificial neural networks. In: 2019 AEIT international conference of electrical and electronic technologies for automotive (AEIT AUTOMOTIVE). IEEE, pp 1–5
33. Zhang S, Zhai B, Guo X et al (2019) Synchronous estimation of state of health and remaining useful lifetime for lithium-ion battery using the incremental capacity and artificial neural networks. *J Energy Storage* 26:100951
34. Chang C, Liu Z, Huang Y et al (2014) Estimation of battery state of health using back propagation neural network. *Comput Aided Draft Des Manuf* 24:60
35. Zhang S, Hosen MS, Kalogiannis T et al (2021) State of health estimation of lithium-ion batteries based on electrochemical impedance spectroscopy and backpropagation neural network. *World Electr Veh J* 12(3):156
36. Chang C, Wang Q, Jiang J et al (2021) Lithium-ion battery state of health estimation using the incremental capacity and wavelet neural networks with genetic algorithm. *J Energy Storage* 38:102570
37. Jianfang J, Keke W, Xiaqiong P et al (2021) Multi-scale prediction of RUL and SOH for lithium-ion batteries based on WNN-UPF combined model. *Chin J Electron* 30(1):26–35
38. Zhang J, Gao XP, Li YQ (2012) Efficient wavelet networks for function learning based on adaptive wavelet neuron selection. *IET Signal Proc* 6(2):79–90
39. Xia B, Cui D, Sun Z et al (2018) State of charge estimation of lithium-ion batteries using optimized Levenberg–Marquardt wavelet neural network. *Energy* 153:694–705
40. Chang WY, Chang PC (2018) Application of radial basis function neural network, to estimate the state of health for LFP battery. *Int J Electr Electron Eng: IEEE* 7(1):1–6
41. Shu X, Shen J, Li G et al (2021) A flexible state-of-health prediction scheme for lithium-ion battery packs with long short-term memory network and transfer learning. *IEEE Trans Transp Electrif* 7(4):2238–3224
42. Liu Q, Kang Y, Qu S et al (2020) An online SOH estimation method based on the fusion of improved ICA and LSTM. 2020 IEEE/IAS Industrial and Commercial Power System Asia (I&CPS Asia). IEEE, pp 1163–1167
43. Gers FA, Schmidhuber J, Cummins F (2000) Learning to forget: continual prediction with LSTM. *Neural Comput* 12(10):2451–2471
44. Kim S J, Kim S H, Lee H M, et al (2020) State of health estimation of li-ion batteries using multi-input LSTM with optimal sequence length. In: 2020 IEEE 29th international symposium on industrial electronics (ISIE). IEEE, pp 1336–1341
45. Shu X, Li G, Shen J et al (2020) A uniform estimation framework for state of health of lithium-ion batteries considering feature extraction and parameters optimization. *Energy* 204:117957
46. Li X, Yuan C, Wang Z (2020) State of health estimation for Li-ion battery via partial incremental capacity analysis based on support vector regression. *Energy* 203:117852
47. Li X, Wang Z, Yan J (2019) Prognostic health condition for lithium battery using the partial incremental capacity and Gaussian process regression. *J Power Sources* 421:56–67
48. Yi Z, Chen Z, Yin K et al (2023) Sensing as the key to the safety and sustainability of new energy storage devices. *Prot Control Mod Power Syst* 8(1):1–22. <https://doi.org/10.1186/s41601-023-00300-2>

49. Wang Z, Yuan C, Li X (2020) Lithium battery state-of-health estimation via differential thermal voltammetry with Gaussian process regression. *IEEE Trans Transp Electrif* 7(1):16–25
50. Yang D, Zhang X, Pan R et al (2018) A novel Gaussian process regression model for state-of-health estimation of lithium-ion battery using charging curve. *J Power Sources* 384:387–395
51. Liu Y, Pu H, Sun DW (2021) Efficient extraction of deep image features using convolutional neural network (CNN) for applications in detecting and analysing complex food matrices. *Trends Food Sci Technol* 113:193–204
52. Szu HH, Telfer BA, Kadambe SL (1992) Neural network adaptive wavelets for signal representation and classification. *Opt Eng* 31(9):1907–1916
53. Saha and B, Goebel K (2007) Battery Data Set, NASA ames prognostics data repository. NASA Ames Research Center
54. He YJ, Shen JN, Shen JF et al (2015) State of health estimation of lithium-ion batteries: a multiscale Gaussian process regression modeling approach. *AIChE J* 61(5):1589–1600
55. Lin C, Xu J, Shi M et al (2022) Constant current charging time based fast state-of-health estimation for lithium-ion batteries. *Energy* 247:123556
56. Choi Y, Ryu S, Park K et al (2019) Machine learning-based lithium-ion battery capacity estimation exploiting multi-channel charging profiles. *IEEE Access* 7:75143–75152
57. Zhou D, Yin H, Fu P et al (2018) Prognostics for state of health of lithium-ion batteries based on Gaussian process regression. *Math Probl Eng* 2018:1–11

**Publisher's Note** Springer Nature remains neutral with regard to jurisdictional claims in published maps and institutional affiliations.